Static and dynamic behavior of a nematic liquid crystal in a magnetic field. Part II : Dynamics

P. Pieranski, F. Brochard, E. Guyon

Classification
Physics abstracts :
14.82

STATIC AND DYNAMIC BEHAVIOR OF A NEMATIC LIQUID CRYSTAL IN A MAGNETIC FIELD

PART II : DYNAMICS

P. PIERANSKI, F. BROCHARD and E. GUYON

Laboratoire de Physique des Solides, Université Paris-Sud, Centre d'Orsay, 91, Orsay

(*Reçu le 13 juillet 1972*)

Résumé. — Nous étudions la dynamique de la transition de Freedericksz d'un cristal liquide nématique orienté, en champ magnétique perpendiculaire. Les techniques thermiques et optiques utilisées ici nous ont déjà permis une description des propriétés d'équilibre de cette transition. Les mesures de taux de relaxation conduisent à une vérification de la théorie hydrodynamique de Leslie-Ericksen, en particulier des effets de couplages hydrodynamiques. La divergence du temps caractéristique au voisinage du champ critique suit de façon remarquable la description de Landau des transitions de phase du deuxième ordre. Les expériences conduisent à une mesure du coefficient de viscosité γ_1.

Abstract. — The dynamics of the distortion of a well-oriented nematic liquid crystal film in a perpendicular field around the Freedericks critical field value is studied both theoretically and experimentally. The experimental thermal and optical techniques have already been used for the description of the equilibrium properties of the transition. Their use for the measurement of transition rates leads to an accurate verification of the Leslie-Ericksen hydrodynamic theory and to a demonstration of the role of back flow effects. The divergence of the characteristic time close to the critical value follows accurately the general Landau model of second order phase transitions. The value of the twist viscosity coefficient γ_1 is obtained.

1. **Introduction.** — In a first article [1] (which we will refer to as I), we have discussed the static behavior, in a magnetic field perpendicular to its director axis **n**, of a nematic film of thickness d contained between two parallel glass plates. The three geometries used were given in figure 1 of I and are reminded in the insert of figure 7. A theoretical discussion based on the Frank Oseen [2] theory leads to the prediction of the existence of a critical field H_c above which the liquid crystal (LC) gets distorted :

$$H_{c_i} = \frac{\pi}{d}\sqrt{\frac{K_{ii}}{\chi_a}}$$

where K_{ii} is an elastic constant and χ_a is the anisotropic part of the magnetic susceptibility.

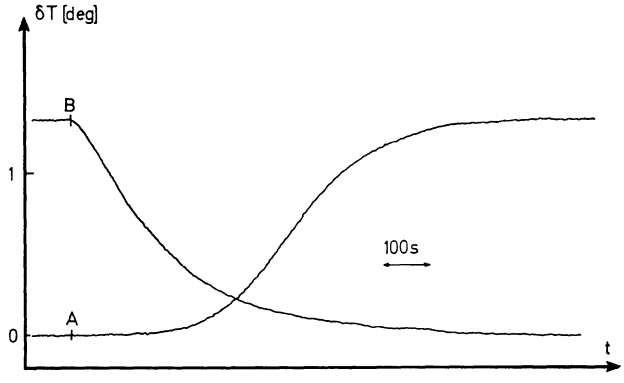

FIG. 1. — Recording of the change of temperature in an homeotropic sample under the influence of a field. At point A, the undistorted film was submitted to a field $H_1 > H_c$. After the equilibrium was reached, the field was decreased at point B to a value $H_2 < H_c$ and an exponential decay is observed. $\delta T > 0$ corresponds to a decrease of the effective heat conductivity.

We have used methoxybenzilidene butylanilin (MBBA) which is in a nematic state between 16 and 46 °C. Our experiments based on heat conductivity and birefringence measurements are carried out in geometries I and III (some results have also been given in the case of geometry II [3]).

In this second article, we consider the dynamic relaxation of the distortion when a field is varied suddenly. A first discussion was given in reference [4] (II). The theoretical description of this behavior will be given in terms of the Leslie Ericksen [5] hydrodynamics theory (we use the notations of ref. [6]).

2. **Experiments.** — 2.1 THERMAL MEASUREMENTS. — The techniques used were described in I. It is to be noted that, in general, the thermal time constant τ_{th} is short enough compared to the distortion time constant

so that dynamic measurements using this technique are meaningful. Typically [7] :

$$\tau_{th}^{-1} \sim \frac{k}{\rho c}\left(\frac{\pi}{d}\right)^2$$

(k is the thermal conductivity, ρ is the specific mass, c is the heat capacity per unit volume). This leads to τ_{th} of the order of 1 s for a 300 μ thick LC film.

Figure 1 shows the variation δT with field of the temperature difference across a 300 μ thick homeotropic (geom. I) LC film. At point A, the undistorted film is subjected to a magnetic field

$$H_1\left(h_1 = \frac{H_1}{H_c} > 1\right).$$

The temperature gradient increases since the heat conductivity along the molecules is larger than that at right angle to them (ref. [1]). At point B, when the equilibrium distorted state has been reached, the field is decreased to a value H_2 ($h_2 = \frac{H_2}{H_c} < 1$). The characteristic times are indeed very large compared to τ_{th}.

2.2 Optical measurements — Figure 2 gives a schematic description of the optical birefringence technique used. A narrow laser beam polarized at 45° to the x axis of an homeotropic LC film enters at right angle with the film : when a field $H > H_c$ is applied along ox, a difference l is introduced in the optical paths of the ordinary beam polarized along oy and the extraordinary one. Assuming a linear propagation along oz, we have :

$$l = \int_{d/2}^{d/2} (n_{eff}(z) - n_0)\, dz$$

where n_0 is the ordinary index, n_e the extraordinary one and n_{eff} is determined from the equation :

$$\frac{1}{n_{eff}^2} = \frac{\cos^2\theta}{n_0^2} + \frac{\sin^2\theta}{n_e^2}.$$

The difference $n_e - n_0$ is generally small

$$\left(\frac{n_e - n_0}{n_0} \sim 15\ \%\right)$$

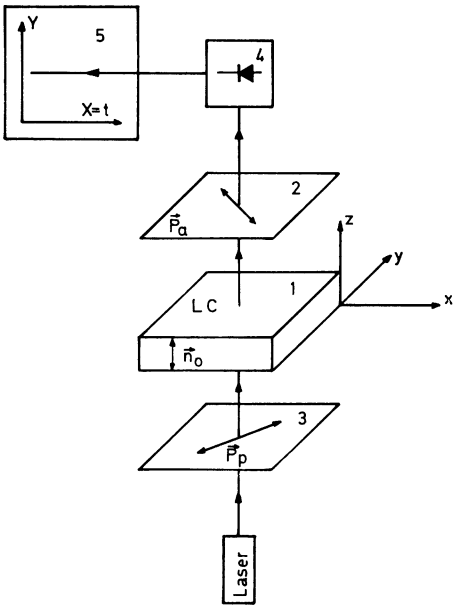

FIG. 2. — Optical set-up used to measure the birefringence of a LC film (1). By adding a condensing lens below the LC, a conoscopic image is observed in the plane of the photocell (4). In geometries I and III, H and $\mathbf{n}_0$ are in the xz plane.

and we can expand $n_{eff} - n_0 = (n_e - n_0)\sin^2\theta$. If we further assume the limit of small distortions (the maximum distortion $\theta_m \ll 1$) and a variation $\theta(z) = \theta_m \cos(\pi z/d)$, we get approximately a phase difference :

$$\delta = 2\pi N = \frac{2\pi l}{\lambda} = \frac{\pi d}{\lambda}\theta_m^2(n_e - n_0)\ (*). \quad (II.1)$$

(*) Let us note that if we had considered the more complex distortions which occur in dynamic experiments (see chapter III), we would still have obtained a form :

$$\delta(t) = G\theta_m^2(t)$$

where G is an undetermined function of the distortions but where all dynamical dependence of θ_m is included in that of δ.

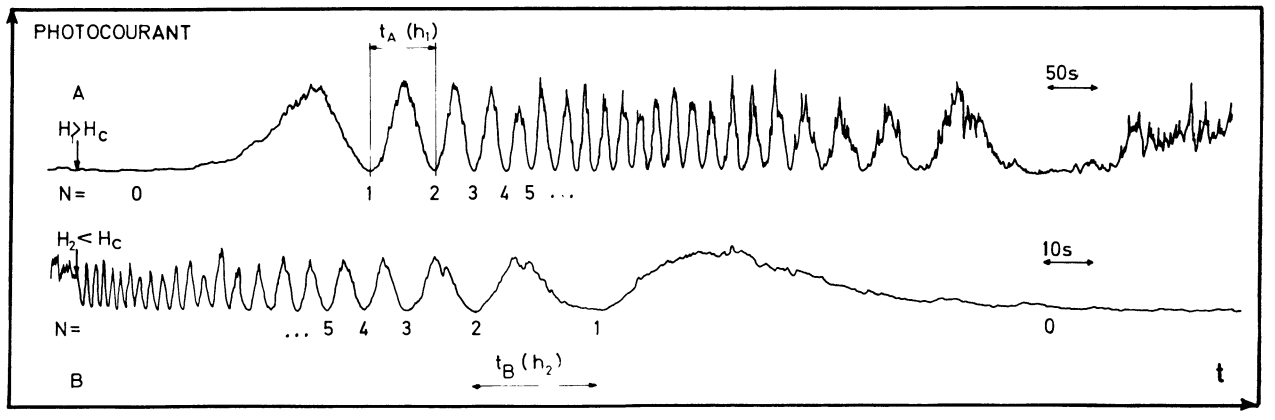

FIG. 3. — Recording of an optical experiment corresponding to the thermal one of figure 1. Note that the order of the extinction fringe, N, is proportional to θ_m^2, as δT in figure 1. The variations obtained in the two cases are equivalent.

The undistorted state corresponds to $\delta = 0$. For a 330 μ thick film, the first order fringe ($N = 1$) (using a monochromatic light $\lambda = .63$ μ, with $n_0 = 1.5$, $n_e = 1.7$) corresponds to $\theta_m^2 = 2 \times 10^{-2}$.

An analyzer (2) is positionned at right angles to the polarizer (1). A photodiode (4) records the variation of intensity between maxima $\delta = (2n + 1)\pi$ and extinctions. In the optical measurements, as well as in the thermal ones, a quantity proportional to the square of the distortion angle is measured.

We show on figure 3 a typical recording of a dynamic optical experiment corresponding to the thermal on of figure 1. We find again an exponential increase of the distortion just above point A and a saturation for larger times whereas the behavior above point B indicates an exponential decay law.

The exponential behavior observed for small distortions can be described for both cases by the relations :

$$N(t) = \alpha\theta_m^2(t) = \alpha\theta_m^2(0) \exp \frac{t}{\tau_{A,B}}(h) \qquad \text{(II.2)}$$

case A t small $\tau_A(h) > 0$,

case B t large $\tau_B(h) < 0$.

Measuring the time difference t_N between two successive extinctions $N + 1$ and N, a value of the time constant $\tau_{A,B}$ is obtained :

$$\tau_{A,B}(h) = \frac{(t_N)_{A,B}}{\text{Log}\dfrac{N+1}{N}}. \qquad \text{(II.3)}$$

We usually measure the time interval $t_A(h_1)$ and $t_B(h_2)$ between the first two fringes ($N = 1$) as indicated on figure 3. In a typical run, because of the long time constants, the field was changed from a value h_1 to h_2 long before the distorted equilibrium state was reached (see Fig. 2 of II). An analysis of these results will be given in chapter IV.

2.3 Discussion. — The optical technique is superior to the thermal one for several reasons.

2.3.1 By using a condenser lens below the LC, one can observe in the plane of the photodiode the conoscopic image given by the sample. We thus could control the quality of the sample (see ref. [1]).

2.3.2 The direct observation of the sample is very useful if one wants to makes sure to work with single domain samples. We remind that, in the presence of a perpendicular field, $\pm\,\theta_m$ distortions are equivalent ; thus, in order to « nucleate » large domains, we initially apply a slightly inclined field and study the dynamical behavior without coming back exactly to the undistorted state.

2.3.3 The limit of small distortions, corresponding to our theoretical discussion, is easily obtained experimentally : the accuracy on the determination of the number of the interfringe N of .1 ; for a 330 μ thick film, it corresponds to an uncertaincy on θ_m^2 : $\Delta\theta_m^2 \sim 10^{-3}$.

2.3.4 The time constant is obtained from a single measurement of a time difference between two consecutive extinctions.

2.3.5 The thermal experiments are difficult to use for long times where the thermal drift becomes important as well as for short times constants (role of τ_{th}).

So, we will use the thermal descriptions only to characterize qualitatively the experimental behavior, the optical ones for the quantitative analysis.

Let us also note that the quality of the optical measurements in the homeotropic geometry is higher than in the planar case : First, the initial alignment seems to be more perfect. Secondly, the distortion is measured starting from a value $N = 0$. In the planar case, the undistorted state corresponds to a maximum value of $\delta = (n_e - n_0)\,d$. Small temperature fluctuations will induce changes of N in the absence of distortion. We have used planar experiments to control the temperature stability of the cell and to study the temperature dependence of the birefringence in agreement with the results of (8) [9].

3. **Theory.** — 3.1 Introduction. — The energy E of a nematic film is a function of the field and of the distortion. In the limit of a small static distortion, $\theta = \theta_m \cos qz$, the results of I (Chap. III) can be summarized as :

$$E_{cm^2} = \frac{1}{2} K_{ii}\, q^2\, d \left[(1 - h^2)\frac{\theta_m^2}{2} + \frac{1}{2}(\eta_i + 1)\frac{\theta_m^4}{4} + \cdots\right]$$

where $i\,(= 1, 2, 3)$ refers to the geometry (insert of

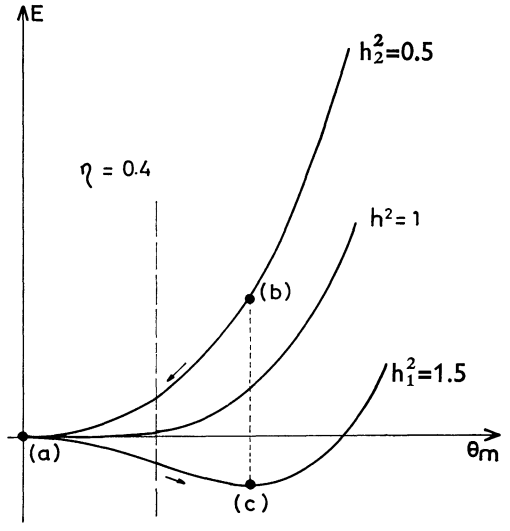

Fig. 4. — Variation of the free energy E versus θ when $H \lesseqgtr H_c$. When a field $h_1 > 1$ is applied to the undistorted film, fluctuations of the orientation are needed to induce the transition form the metastable equilibrium state (*a*) to the final state (*c*). The relaxation from point (*b*), when the field is decreased to avalue $H_2 < H_c$, is much faster (see Fig. 1) than the increase from point (*a*). The limit of small distortions corresponds to the left of the broken line where only the lowest order contribution is considered.

Fig. 7) and η_i measures the anisotropy of the elastic constants K :

$$\eta_1 = \frac{K_{33} - K_{11}}{K_{11}}, \quad \eta_2 = 1, \quad \eta_3 = \frac{K_{11} - K_{33}}{K_{33}}.$$

The variation of E with θ_m is shown schematically on figure 4. Starting from an undistorted state (a), a field H_1 ($h_1 > 1$) is applied and the system evolves to an equilibrium distorted state (c). Point (a) corresponds to a metastable state of the system. The initial distortions or fluctuations of the orientation induce the transition to the stable state (c). This explains the slow increase of the distortion above point A in figure 1 and 3. When the field is suddenly decreased ($c \to b$) to a value H_2 ($h_2 < 1$), point b is not a stable state of the system and the distortion relaxes rapidly to the undistorted state a. The rate of change of $\theta_m(t)$ depends on that of E as θ varies and on hydrodynamic backflow effects. The limit of small distortions corresponds, in figure 4, to the left of the broken line where only the quadratic (harmonic) variations of $E(\theta)$ are taken into account.

3.2 GEOMETRY 2. — We consider this case first because only one elastic constant is involved and because no hydrodynamic motion results from the torsion of the director (one can apply a torsion to the configuration without changing the positions of the centers of the molecules).

3.2.1 *Application of a field* $H_1 \gtrsim H_c$. — Using the notations of, reference [6], the equilibrium between the elastic and the viscous torques (expressed in terms of the viscosity facteur γ_1) can be written as :

$$K_{22} \frac{\partial^2 \theta}{dz^2} + \sin\theta \cos\theta \, \chi_a H_1^2 = \gamma_1 \frac{\partial \theta}{\partial t}. \quad \text{(III.1)}$$

When

$$\frac{H_1 - H_c}{H_c} \ll 1,$$

θ is small and (III.1) becomes :

$$\xi_2^2 \frac{\partial^2 \theta}{\partial z^2} + \theta - \frac{2}{3}\theta^3 = \lambda \frac{\partial \theta}{\partial t}. \quad \text{(III.2)}$$

Here $\lambda = \dfrac{\gamma_1}{\chi_a H_1^2}$ and $\xi_2^2 = \dfrac{K_{22}}{\chi_a H_1^2}$.

The most general solution of (2), which satisfies the boundary conditions $\theta(\pm d/2) = 0$, is

$$\theta = \sum_n c_n(t) \cos(2n + 1)\frac{\pi z}{d}$$

with $| c_n(t) | \ll 1$.

Multiplying eq. (III.2) by $\cos(2n + 1)\pi z/d$ and performing the integration over z, one obtains a set of differential equations for $c_n(t)$. For $n = 1$, one sees easily that the anharmonic term c_1 is of the order of c_0^3. So, with a good approximation, we can take the solution of (III.2) as

$$\theta = \theta_m(t) \cos\frac{\pi z}{d}$$

where the maximum distortion angle, $\theta_m(t)$, obeys the fundamental relation to be used in the following :

$$\left[1 - \left(\frac{H_c}{H_1}\right)^2\right]\theta_m - \frac{\theta_m^3}{2} = \lambda \frac{d\theta_M}{dt}. \quad \text{(III.3)}$$

This equation can be integrated as :

$$\theta_m^2(t) = \frac{\theta^2(\infty)}{1 + \left(\dfrac{\theta^2(\infty)}{\varepsilon^2} - 1\right)\exp\left[-\dfrac{2\chi_a H_c^2}{\gamma_1}(h_1^2 - 1)\, t\right]}. \quad \text{(III.4)}$$

Physically $\theta_m^2(t)$ is just proportional to the time dependent contribution of the heat conductivity. Actually, the experimental variation of $\delta T(t)$, when a field is applied, given on figure 1, has the same characteristic shape as the solution of (III.4) given on figure 5 for a typical set of parameters ($\varepsilon^2 = 10^{-5}$, $h_1 = 1.25$) :

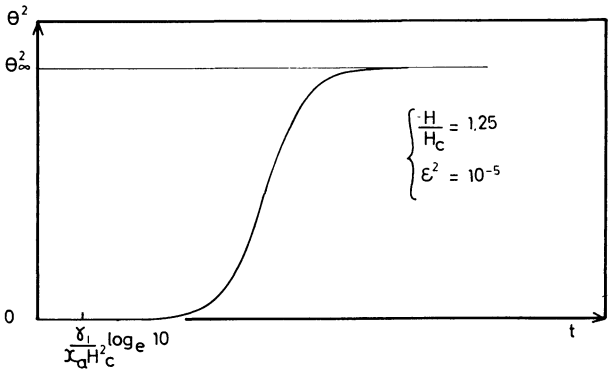

FIG. 5. — Calculation of the increase of $\theta_m^2(t)$ in the evolution from (a) to (c) in the case of geometry II (compare to Fig. 1*A*). The saturation of the distortion comes from the higher order terms in the free energy expansion which also determine the equilibrium distortion.

For *large values of* t, $\theta_m(t)$ reaches the saturated value $\theta(\infty)$ exponentially with a time constant $s_0^{-1}(h)$:

$$s_0(h) = \frac{\chi_a H_c^2}{\gamma_1}(h^2 - 1).$$

For *small values of* t, the initial increase of the distortion is given by :

$$\theta_m^2(t) = \varepsilon^2 \exp[2\, s_0(h)\, t].$$

The fluctuations of the orientation in the undistorted state ($t = 0$) are represented by the average :

$$\varepsilon^2 = < \theta_m^2 (t = 0) > .$$

In order to obtain the thermal contribution to ε^2, we apply the equipartition theorem. The fluctuations of the director axis around the average value of $\mathbf{n}$ will be described by $\delta\mathbf{n}(r)$. Their Fourier components are given by :

$$\delta\mathbf{n} = \sum_n \sum_{q_\parallel} \delta n_q \cos(2n + 1)\frac{\pi z}{d} \exp(i\mathbf{n}_\parallel \mathbf{r}) .$$

The wave vector $\mathbf{q}$ has a quantized component along oz and a continuous component in the plane of the film, $\mathbf{q}_\parallel$.

Let us consider the limiting case where the elastic constants are equal. $K_{ii} = K$. The free energy becomes :

$$F = \frac{V}{2} \sum_{n,q_\parallel} K[\delta n_y^2(q_\parallel^2 + q_z^2 - \chi_a H_l^2) + \delta n_z^2(q_\parallel^2 + q_z^2)] .$$

V is the volume of the sample and H_l ($> H_c$) is the initial, lower value of the field, before the upper field H_1 ($> H_c$) is applied [the magnetic field is parallel to oy].

In thermal equilibrium, we have :

$$< \delta n_y^2 > = \frac{kT}{V[K(q_\parallel^2 + q_z^2) - \chi_a H_l^2]}$$

$$< \delta n_z^2 > = \frac{kT}{V[K(q_\parallel^2 + q_z^2)]} .$$

The equation of evolution of a fluctuation

$$\theta = \theta_q \cos\frac{\pi z}{d} \exp(i\mathbf{q}_\parallel \mathbf{r})$$

is :

$$\xi^2 \theta_q(\kappa^2 - q_\parallel^2) = \lambda \frac{d\theta_q}{dt} \qquad \text{(III.5)}$$

where

$$\kappa = \frac{1}{\xi(H_1)} \left(1 - \left(\frac{H_c}{H_1}\right)^2\right)^{1/2} .$$

The characteristic length for the fluctuations in a plane perpendicular to oz, κ^{-1}, diverges at the phase transition at H_c. The effect of this divergence might be observed in light scattering experiments.

Eq. (II.5) shows that only the fluctuations $q_z = \pi/d$ and $q_\parallel < \kappa$ become unstable when H_1 is applied. Thus ε^2 is calculated by summing δn_y^2 from the upper bound $q_\parallel \sim \kappa$ to $q_\parallel = \pi/L$ (the characteristic dimension of the sample perpendicular to z, L, gives a lower cut off).

$$\varepsilon^2 = \frac{kT}{VK} \int_{\pi/L}^{\kappa} \frac{2\pi q_\parallel \, dq_\parallel \, S/(2\pi)^2}{\mu^2 + q_\parallel^2}$$

with

$$\mu = \frac{\pi}{d} \left(1 - \left[\frac{H_l}{H_c}\right]^2\right)^{1/2} .$$

As H_l gets close to H_c, ε^2 shows a weakly singular behavior

$$\varepsilon^2 = \frac{kT}{2\pi \, dK} \cdot \mathrm{Log}\left(1 + \frac{h_1^2 - 1}{1 - h_l^2}\right) \qquad \text{(III.6)}$$

(we have neglected the effect of the lower cut off π/L which would prevent the divergence of ε^2 if h_l became extremely close to 1).

3.2.2 *Suppression of a field.* — The equilibrium between the elastic and viscous torques can be expressed as :

$$K_{22} \frac{\partial^2\theta}{\partial z^2} = \gamma_1 \frac{\partial\theta}{\partial t} . \qquad \text{(III.7)}$$

The angle θ varies exponentially with time, with the decay characteristic time constants $\tau_0, \tau_1, \ldots, \tau_n$:

$$\frac{1}{\tau_n} = \frac{K_{22}}{\gamma_1} \left[\frac{(2n + 1)\pi}{d}\right]^2 .$$

If H is large compared to H_c, $\theta(z)$ is a mixture of eigenfunctions. But the time τ_0 ($= 9\tau_1 = 25\tau_2$) gives the slowest decay corresponding to the least distorted solution. $\theta(t)$ will obey a simple exponential law, $\exp\left(-\frac{t}{\tau_0}\right)$ typically as soon as $t > \tau_1$.

3.2.3 *Differential relaxation time.* — We study the relaxation of the system for small variations δ around the equilibrium value of the angle, θ, in the presence of a field H.

1° $H \gtrsim H_c$. — The equilibrium value $\theta_m(\infty)$ is given by the eq. (IV.3) of I :

$$\theta_m^2(\infty) = 2\left[1 - \left(\frac{H_c}{H}\right)^2\right] .$$

The evolution of $\theta_m(t) = \theta_m(\infty) + \delta$ is obtained by eq. (III.3) around $\theta_m(\infty)$:

$$-2\left[1 - \left(\frac{H_c}{H}\right)^2\right]\delta = \lambda \frac{d\delta}{dt} \qquad \text{(III.8)}$$

δ decreases exponentially with a time constant :

$$\tau_d^{-1} = \frac{2\chi_a H_c^2}{\gamma_1}(h^2 - 1) \qquad \text{(III.9)}$$

already obtained in paragraph 3.2.1.

2° $H < H_c$. — When H is below H_c, $\theta_m(\infty) = 0$ and eq. (III.3) becomes :

$$\left[1 - \left(\frac{H_c}{H}\right)^2\right]\delta = \lambda \frac{d\delta}{dt}$$

δ decays exponentially again with a time constant :

$$\tau_d^{-1} = \frac{\chi_a H_c^2}{\gamma_1}(1 - h^2) . \qquad \text{(III.10)}$$

The relaxation times below and above H_c are in a two to one relationship. However, the physical parameter

measured in our experiments is proportional to θ^2 and varies as $2\,\delta\theta$ in the first case and as δ^2 in the second case. Thus, the two measured characteristic times should be given with the same factor 2.

3° $H \gg H_c$. — The LC is almost completely aligned along H. The stable configuration corresponds to $\theta = \pi/2$. The equation of motion for

$$\theta = \frac{\pi}{2} - \delta(z, t)$$

becomes :

$$- K_{22} \frac{\partial^2 \delta}{\partial z^2} + \chi_a H^2 \delta = - \gamma_1 \frac{\partial \delta}{\partial t}$$

δ varies exponentially in time. The slowest process is given by :

$$\frac{1}{\tau_d} = \frac{\chi_a H_c^2}{\gamma_1}(1 + h^2)\,. \qquad \text{(III.11)}$$

3.3 GEOMETRY I AND III. — The problem is more delicate for these two cases : two elastic constants (K_{11} and K_{33}) appear in the description ; an hydrodynamic motion results from the torsion of the molecules. This is shown schematically on figure 6.

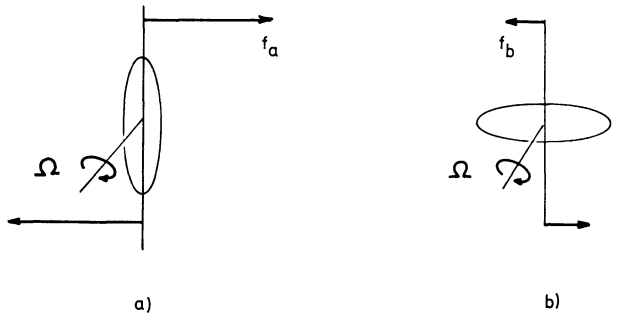

FIG. 6. — In the presence of the rotation of the molecules with an angular velocity Ω, the torque acting on an elementary volume of the fluid [10] is $f_a = \frac{\gamma_1 - \gamma_2}{2}\,\Omega$, $f_b = \frac{\gamma_1 + \gamma_2}{2}\,\Omega$; usually $| f_a | \gg | f_b |$. For a weakly distorted LC, the back flow effects are much larger in the homeotropic case (*a*) than in the planar (*b*).

The resulting backflow torque has been calculated in (10). It is important in the homeotropic case (case *a*). In pratice, it is small in the planar geometry (case *b*) and the dynamical behavior for small distortions will be similar to that described in B for geometry II. (Yet we make a complete discussion of geometry I as this is not necessarily always the case.) However, for large fields, the orientation of the molecules in the central part of the film is at right angle with the initial orientation and the backflow effects should be more important for a planar film than for an homeotropic one.

We will restrict our theoretical analysis as well as a quantitative discussion of our experiments to the limit of small distortions. The problem is expressed in terms of the following equations :

3.3.1 The gradient of the angular velocity of **n** induces a backflow motion causing a frictional torque on **n** :

$$\mathbf{\Gamma}' = \mathbf{n} \wedge \gamma_1(- \boldsymbol{\omega} \wedge \mathbf{n}) + \gamma_2 \bar{\bar{A}}\mathbf{n}$$

with $2\,\omega = \text{curl}\, v$ and

$$2\,A_{ij} = \left(\frac{\partial v_i}{\partial x_j} + \frac{\partial v_j}{\partial x_i}\right).$$

Due to the quasi infinite planar geometry, and if we neglect compressibility effects, the only non zero component of **v** is $v_x(z, t)$. The equilibrium between elastic, magnetic and viscous torques can be written as :

$$\xi_i^2 \frac{\partial^2 \theta}{\partial z} + \theta = \lambda \frac{\partial \theta}{\partial t} + \lambda\lambda_i \frac{\partial V_x}{\partial z} \qquad \text{(III.12)}$$

with

$$\lambda_1 = \frac{\gamma_1 + \gamma_2}{2\,\gamma_1}, \quad \lambda_3 = \frac{\gamma_2 - \gamma_1}{2\,\gamma_1}.$$

For MBBA, the ratio λ is small [11]. Once more we meet the fact that the hydrodynamic coupling is weak in the planar geometry and this equation becomes equivalent to the linearized formula III.

3.3.2 the gradient $\partial V_x/\partial z$ is related to the angular velocity of **n** by the Leslie equation of the hydrodynamic motion [5], [6]. Neglecting the inertial effects, correct here, this equation can be written as :

$$\frac{\partial}{\partial z}\left(a_i \frac{\partial V_x}{\partial z} + b_i \frac{\partial \theta}{\partial t}\right) = 0 \qquad \text{(III.13)}$$

$$a_1 = \eta_1 = \frac{1}{2}(\alpha_4 + \alpha_6 + \alpha_3) \quad b_1 = \alpha_3$$

$$a_3 = \eta_2 = \frac{1}{2}(\alpha_4 + \alpha_5 - \alpha_2) \quad b_3 = \alpha_2\,.$$

The coefficients η_1 and η_2 represent the kinematic viscosity for a shear flow $V_x(z)$ parallel and perpendicular to **n** as measured initially by Miesowicz [12].

The Leslie coefficients have been obtained for MBBA by Gähwiller [11]. The coupling between the rotation of the molecules and the velocity depends on the geometry. In the planar case where b_1/a_1 is small (~ 0 for MBBA) this coupling is negligible.

3.3.3 The boundary conditions for **n** and for **V** are :

$$\theta\left(\pm \frac{d}{2}\right) = 0 \qquad \text{(III.14}a\text{)}$$

$$V_x\left(\pm \frac{d}{2}\right) = 0\,. \qquad \text{(III.14}b\text{)}$$

If we had considered the static solution

$$\theta = \theta_m(t) \cos \frac{\pi z}{d},$$

eq. (III.13) would have implied a form for v :

$$V_x(z, t) = v_m(t) \sin \frac{\pi z}{d}$$

which does not satisfy (III.14*b*). This means that the evolution of the system does not follow a sequence of quasistatic states. The form of the general solution in a dynamic experiment is more complex :

$$\theta(z, t) = \theta_0 \left(\cos kz - \cos \frac{kd}{2}\right) e^{st} \qquad \text{(III.15}a\text{)}$$

$$V_x(z, t) = V_0 \left(\sin kz - \frac{2z}{d} \sin \frac{kd}{2}\right) e^{st} \qquad \text{(III.15}b\text{)}$$

so that the velocity vanishes as the limiting planes. The time of establishment of the velocity

$$\tau^{-1} = \frac{\pi^2}{d^2} \frac{\eta}{\rho}$$

(corresponding to the « fast modes » of (6)) is much smaller than s^{-1} and can be neglected.

Eq. (III.12) and (III.13) lead to the following conditions for the wave vector of the distortion k and for the time constant s^{-1}

$$(1 - A)\, s\lambda = 1 - \frac{4X^2}{\pi^2 h^2} \qquad \text{(III.16)}$$

$$h^2 = \frac{4X^2}{\pi^2} \frac{\tan X - X/A}{\tan X - X} \qquad \text{(III.17)}$$

where

$$A_i = \frac{\lambda_i b_i}{a_i}, \quad X = \frac{kd}{2} .$$

The number X gives the variation of the wave vector (for the static case, $X = \pi/2$).

In the geometry I, A ($\sim 10^{-3}$) is small for MBBA and the solutions of the coupled eq. (III.16), (III.17) are $X = \pi/2$ and a time constant

$$s_0^{-1}(h) = \frac{\lambda}{1 - \frac{1}{h^2}} = \left[\frac{\chi_a H_c^2}{\gamma_1} (h^2 - 1)\right]^{-1} \qquad \text{(III.18)}$$

as in the case of geometry II.

The results for geometry III, using the value $A = .75$ for MBBA [11], are plotted on figure 7 already given in reference [2].

We have kept the smallest X solution : for positive s, it corresponds to the fastest increase of the distortion (as seen on (III.16)) and, for negative s, to the slowest decrease of the distortion. Curve (*a*) shows that the wave vector of the distortion increases with the field. For $h \sim 1$, the distortion is very slow and we get $X = \pi/2$: As θ varies slowly, a quasistatic variation is naturally expected. The limiting values of the curves are X_0 (tg $X_0 = X_0/A$) and X_1 (tg $X_1 = X_1$). The distortions for different values of h are represented

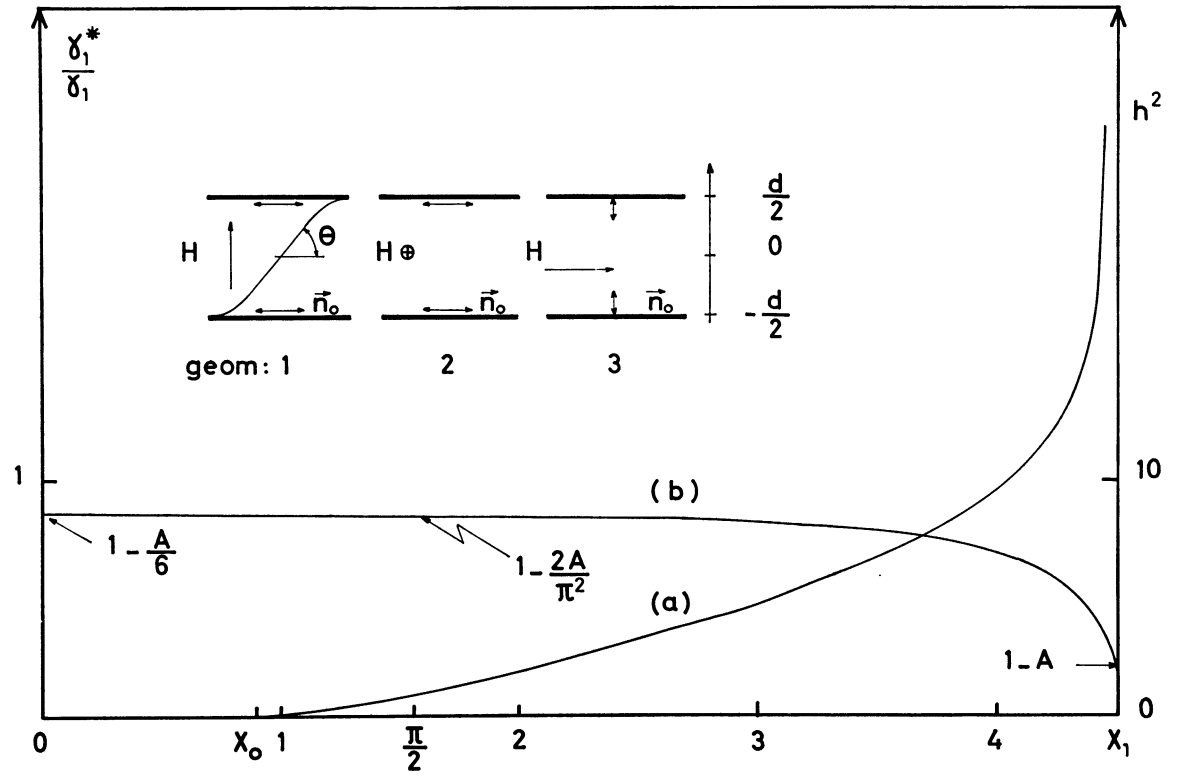

FIG. 7. — The insert gives the 3 geometries used for the study of the Freeder ksz transition (geom. I and III were used in this report). Curve (*a*) in the homeotropic case shows the increase of the wave vector of the distortion $k = 2\ dX$ as the field h increases. Curve (*b*) gives the corresponding decrease of the effective viscosity $\gamma_1^*(h)$.

schematically on figure 8 and are quite different from the static solution.

It should be possible to check the backflow effects directly using, for example, the motion of dust particles in the LC. The relation between V and θ is

$$V_0 = \frac{\alpha_2}{\eta_2 k} s\theta_m .$$

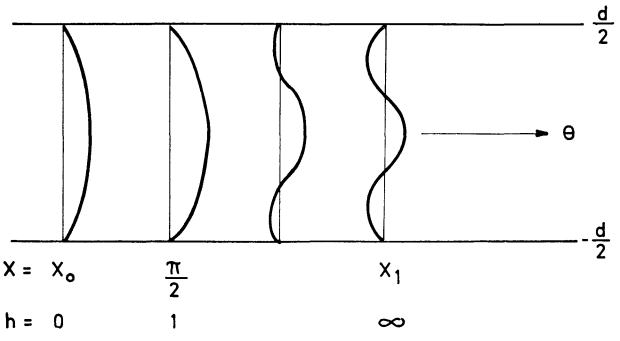

FIG. 8. — Schematic description of the time dependent part of the distortion angle $\theta(z, t)$ for different values of h (corresponding to curve (*a*) of Fig. 7).

The fluid should move on a distance typically

$$\frac{d}{\pi}\theta_m ; \quad \left(\frac{\alpha_2}{\eta_2} \sim 1\right)$$

of the order of magnitude of the thickness.

The variation of the time constant s^{-1} with the field can be expressed by writing

$$s(h) = \frac{\chi_a H_c^2 (h^2 - 1)}{\gamma_1^*(h)} \qquad \text{(III.19)}$$

by analogy with geometry II. The effective viscosity $\gamma_1^*(h)$ is

$$\frac{\gamma_1^*(h)}{\gamma_1} = \frac{s_0(h)}{s(h)} \qquad \text{(III.20)}$$

where $s_0(h)$ is given by (III.18).

The ratio $\gamma_1^*(h)/\gamma_1$ has been calculated in geometry III for MBBA and is given on figure curve *b*. It decreases as h and the distortion increase. The limiting value for large distortions — (1 − A) — turns out to be the value predicted for the decrease of viscosity in shear wave ultrasonic attenuation measurements [13] in an unbounded medium. For smaller distortions, the effect of the backflow, which reduces the viscosity, is not as strong, as the presence of the boundaries limits the variation of V. Even for $h = 0$, γ_1^* remains smaller than the kinematic value γ_1. However, for small fields ($h^2 < 5$), the relative variation of γ_1^* with h is negligible and the dynamic behavior in geometry III should be quite similar to that in the planar case II.

4. Experiments. — 4.1 THERMAL RESULTS. — The experimental effects in the homeotropic and planar case are qualitatively similar and we will discuss at the same time the dynamic behavior for these both geometries.

We use the thermal data to characterize the dynamic behavior in the three situations discussed theoretically : finite increase of field from an undistorted state, finite decrease of field from a distorted initial state, differential changes of field. A quantitative description of the dynamics, in the limit of small distortions, will be given using the optical data.

4.1.1 *Experiments in a decreasing field* ; from an upper value H_u ($> H_c$) to a lower value H_2 ($< H_c$). — Let us consider some typical results put together in figure 9. Starting from an undistorted homeotropic state, we first applied a field, $h_u = 1.8$, then we suppressed it after the equilibrium had been reached (curve 1). In a second experiment (curve 2), the same field was applied but is was turned off before the equilibrium was reached. Finally (curve 3), a lower field, $h = 1.4$, was applied and the decay was observed after the saturation was reached. The decay curves obtained in these three cases are very similar. The comparison between 1, 2 and 3 strongly suggests that, although the field value is turned on or off suddenly, the transition of the LC to the final state follows a sequence of quasi equilibrium states.

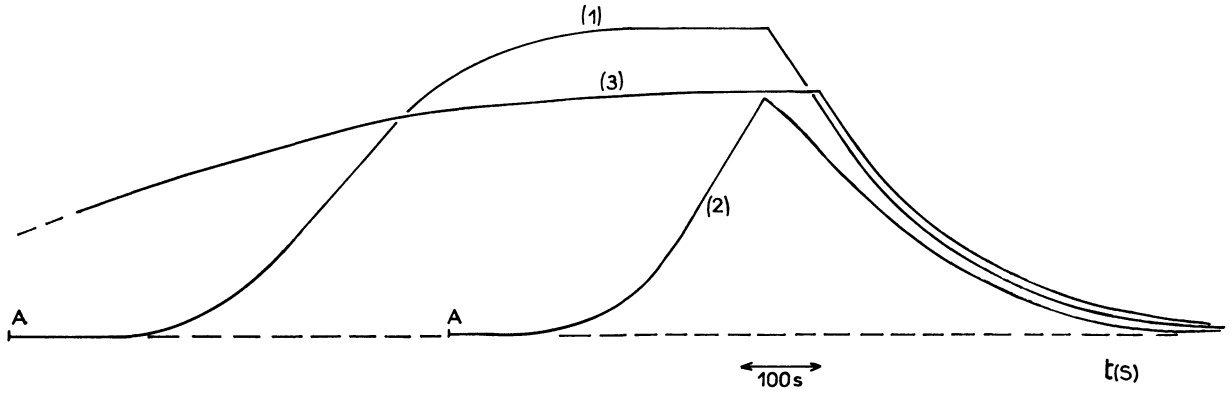

FIG. 9. — The exponential decay of the distortion, measured thermally, when H is decreased to $H_2 < H_c$ does not depend on the initial preparation of the distorted state.

In figure 10, we see that the decay behavior obeys an exponential law over the complete time scale and allows an accurate estimate of the time constants τ_B. This time constant is relatively insensitive to the value of the initial field h_u. (This was already apparent in the comparison of curves 1 and 3 of Fig. 9.) This is a little surprising, considering the results of the theoretical analysis : for small values of H_u, the time constant should depend on K_{33} and the back flow should be large. For large values of H_u, the initial behavior should depend on K_{11} but with a small back flow contribution.

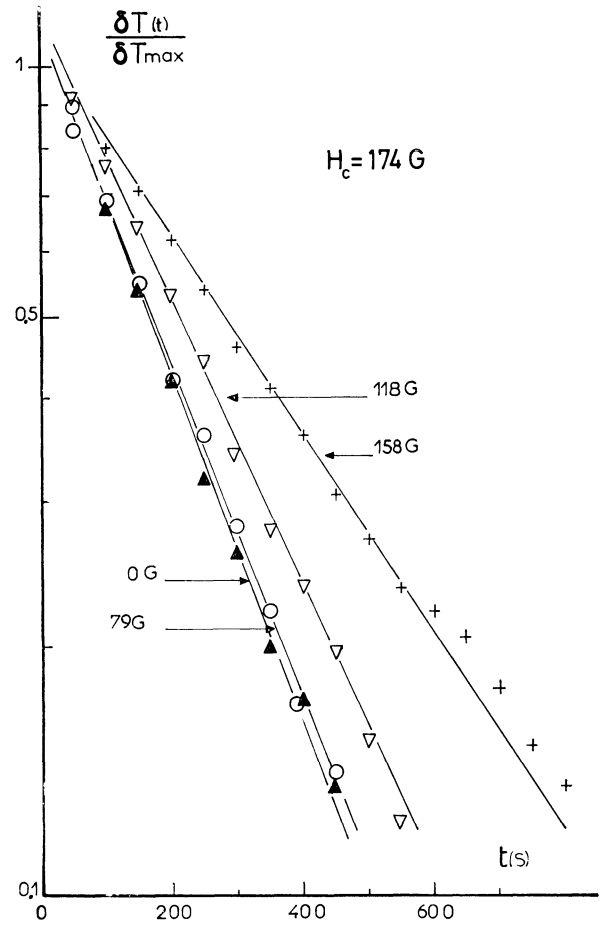

FIG. 10. — The time constant of the exponential relaxation in down field experiments, measured thermally, becomes very long as (H_c — H_2) decreases to zero (H_2 = 0 ; 79 ; 118 ; 158 G).

When the final value of the field H_2 increases, the time constant of the decay increases (see part B). However, when H_2 is close to H_c, the process cannot be described by a single time constant : there is a fast initial decay ; the variation becomes extremely slow for large times. We characterize $\tau_B(h_2)$ from the exponential behavior at large times.

4.1.2 *Experiments in an increasing field.* — We consider the case of a finite jump of field from a lower field h_l (< 1) to h_1 (> 1).

a) Shape of the time variation.

We have already discussed, in the theoretical chapter, the characteristic behavior of the variation of $\delta T(t)$, using the analysis of geometry II.

The shape characterized by formule (III.4) can be conveniently represented by using the coordinates

$$y = \mathrm{Log}\left(\frac{\delta T(\infty)}{\delta T(t)} - 1\right)$$

versus t. If we remind that $\delta T(t)$ is proportional to $\theta_m^2(t)$, we expect a linear variation of $y(t)$. The intercept with the $t = 0$ axis gives the normalized contribution of ε^2, $\theta_m^2(\infty)/\varepsilon^2$. The inverse of the slope measures the time constant τ_A. We will discuss these two terms separately in the following.

The quantity measured is

$$\frac{\delta T(\infty) - \delta T(0)}{\delta T(t) - \delta T(0)},$$

which diverges at $t = 0$, rather than $\delta T(\infty)/\delta T(0)$. A correction was made for $\delta T(0)$ (that is for ε^2) iteratively by plotting first the measured quantity and getting ε^2 from an extrapolation at $t = 0$ of the variation for large times. On figure 11 are given some corrected curves for a value of $h_1 = 1.5$ and different value of h_l which show a linear variation in agreement with expression (III.4). Let us note however that this linear variation $y(t)$ is not well obeyed for large values of h_1 (> 2), outside the domain of validity of the theoretical model given in (III.B).

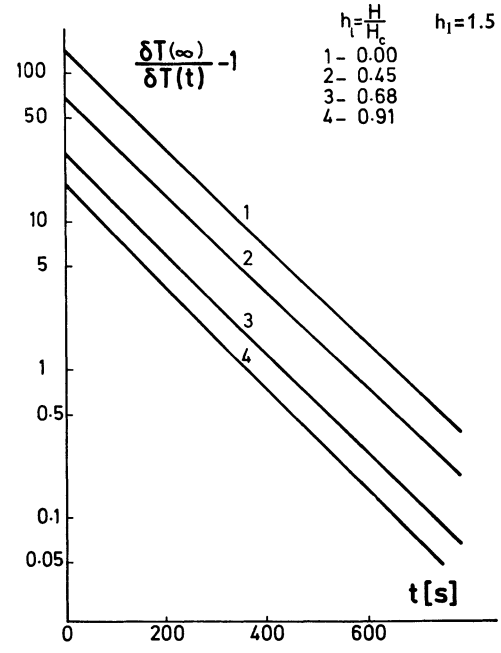

FIG. 11. — Thermal experiment. Curve 1 ; at a time $t = 0$, an upper field $H_1 = 1.5\ H_c$ is applied. Ln $\left(\frac{\delta T(\infty)}{\delta T(t)} - 1\right)$ varies linearly with time in agreement with (III.4). Curves 2, 3, 4 ; the initial distortion has been increased by increasing h_l (> 1). The time constant measured by the slope is unchanged ; ε^2, given by the inverse of the intercept with the $t = 0$ axis, increases.

b) Fluctuations.

We first discuss qualitatively some possible sources of initial misalignment :

— Thermodynamic fluctuations : the contribution was estimated in the theoretical part of this chapter.

— Poor alignment in the initial state. In the experiments reported in a previous note [14], the behavior in an increasing field was very similar to that in a decreasing field. We have given in figure 12 (curve 3) such a typical « upward » field variation. The initial misalignment was rather large due to an insufficient surface treatment (although we could observe extinction along the principal axis between crossed polaroids).

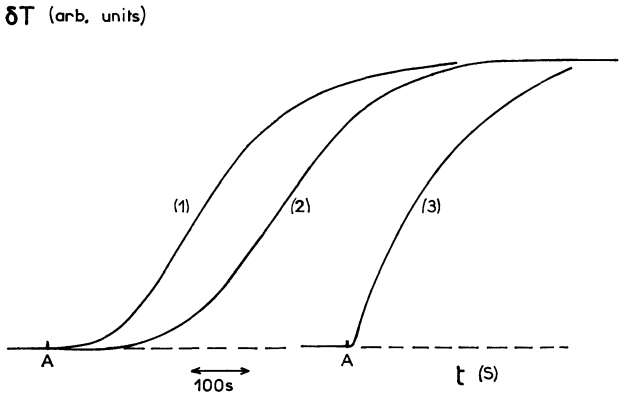

FIG. 12. — Initial distortion for a well aligned planar film in a perpendicular field (2), in a slightly inclined field (1) and for a poorly aligned film (3).

— Tilt of the magnetic field. In an homeotropic sample, we have applied a magnetic field at an angle with *oz*. The curve for a field tilted by an angle of 6° (Fig. 12, curve 1) shows a faster initial start than that with a field perpendicular to *oz* (curve 2). It also indicates that a very large misalignment is probably required to get curve 3. The exponential behaviors of 1 and 2 for large times are very close. De Gennes has suggested to us that the large time behavior could be controlled by the exlusion of walls separating domains with opposite value of the angle, $\pm\,\theta_m$. In the planar case, for example, such a wall would have a heat conductivity smaller than that of an homogeneous region. However, the growth of the + and − domains should depend drastically on the tilting of the field which would favor one sign : the absence of such effects in our experiments may be due to a small residual misalignment and to the fact that the area of the walls is only a small fraction of the total area of our thermal experiments (although we have actually observed these walls in the two configurations studied here).

Let us consider quantitatively the results of figure 11 for different values of the initial lower field h_l (= 0 ; 0.45 ; 0.68 ; 0.91) and the same value of $h_1 = 1.5$. All curves are parallel. This shows that the time constant τ_A is only a function of h_1 as expected from (III.4). The lower curves correspond to the largest values of h_l (on the experimental curves, the initial start of $\delta T(t)$ becomes faster as h_l increases). This effect could either be due to the increased importance of the quadratic angular fluctuations when $h_l \to 1$, discussed in the theoretical chapter, or to that of the distortion in a slightly tilted field. Rapini [15] has considered this effect : If the distortion θ_m ($H = 0$) is non zero, there is no longer a critical field and $\theta_m(H)$ increases continuously with H_l. However, if $\theta_m(0)$ is sufficiently small, the distortion will be negligible up to a quasi critical field. The distortion $\varepsilon^2(0)$ measured in our dynamic experiments is typically 10 times larger than that which would be estimated in the angular fluctuation model and we believe that the Rapini description explains best our results. On figure 13, we present the result of an optical determination of the fringe order $N(t = 0, H_l)$ taken at time $t = 0$ just before the application of an upper field H_1, for a 150 μ homeotropic film. For H_l sufficiently large, $N(0, H_l)$ is given from the integer count of interference fringes : The full line curve represents the static equilibrium data above the Freedericksz field as discussed in I. For low values of H_1, (typically when $N < 1$), $N(0, H_1)$ is obtained from the measurement of the dynamics of the initial increase of distortion :

$$N(t) = N(0) \exp\left(\frac{t}{\tau(H_1)}\right)$$

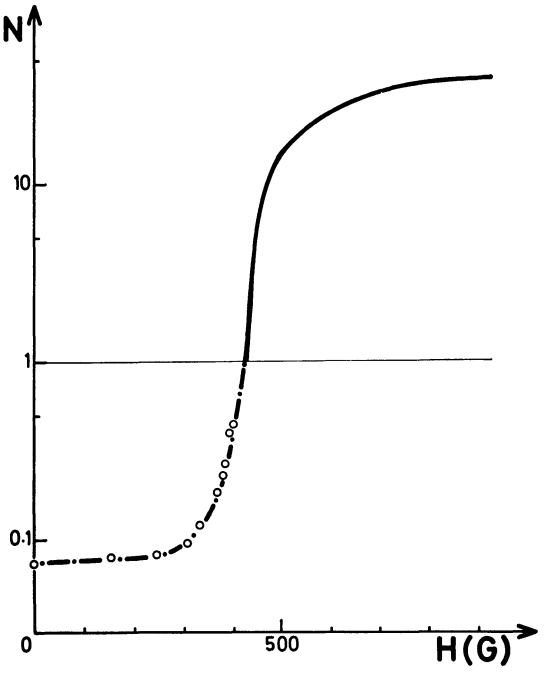

FIG. 13. — Variation of the order number of fringes, $N(\propto \theta_m^2)$ for a well aligned 150 μ homeotropic film in a *nearly* perpendicular field. The distortion for $N > 1$ is measured directly and corresponds to the static results described in I. The experimental values for $N(H) < 1$ are determined from the growth rate in a field H sufficiently lower than H_c. Strictly speaking, there is no more a critical field because of the small initial misalignment (estimated to less than 2°). (Note the Log N scale.)

as obtained from (II.2). The extrapolation of the linear variation of Log N versus t gives $N(0)$. The data points obtained by this technique define a curve (half dotted line) which merges nicely in the full line curve obtained for larger fields. This variation is very similar to that calculated in (15) with $\theta(0)$ of the order of one degree. There is no critical field ; however (note the Log vertical scale) a fast increase of N takes place above a value $H = 450$ G. This first (to our knowledge) accurate measurement of this low field « rounding » has been made possible using the « exponential magnification effect » of the dynamical behavior. This method is remarkable in that is it best suited for the study of very small distortions where the times to be measured are larger.

4.1.3 *Differential behavior.* — In figure 7 of reference 1, we have shown the effect of small temperature changes due to small variations of field around a value $h > 1$. The time variation of δT is exponential with a time constant $\tau_d(h)$. This time is the same whether the field is increased or decreased. When h gets close to 1, this time is found to diverge as $(h - 1)^{-1}$ as obtained in (III.9). In the limit of small distortions, the variation of $\tau_d(h)$, is quite comparable to that of $\tau_{A,B}$ and we will not discuss it in the quantitative analysis of next paragraph.

4.2 Optical data. — Let us first point out that the optical results agree completely with the thermal description. In the limit where θ_m^2 is small, considered in this paragraph, we characterize the time constant $\tau_{A,B}$ of Form (II.2) in the presence of a field increase (A) or decrease (B) from the value of the time interval $t_{A,B}$ given figure 3.

4.2.1 *Field dependence of* $\tau(h)$. — It is characterized from the value of the normalized ratio $t_B(0)/t_B(h)$ for $h < 1$ and $t_B(0)/t_A(h)$ for $h > 1$. If we apply (II.3) and the results of (III.19) and (III.20), we obtain :

$$\frac{t(0)}{t(h)} = \frac{\tau(0)}{\tau(h)} = \frac{\gamma_1^*(0)}{\gamma_1^*(h)}(h^2 - 1)\,. \qquad \text{(IV.1)}$$

The results for several planar samples are plotted on figure 14. They follow closely a $(h^2 - 1)$ law. In particular, the divergence of $\tau(h)$ as $(h - 1)^{-1}$ for $h = 1$, predicted by the Landau model of second order phase transitions [16], is accurately obtained on both sides of the transition as in the superconducting corresponding problem discussed in the appendix. A similar variation was reported in reference [2] for homeotropic films in a field range $0 < h^2 < 5$. This behavior is consistent with the result of Form (IV.I). However, we expect the value of the ratio $\gamma_1^*(0)/\gamma_1^*(h)$

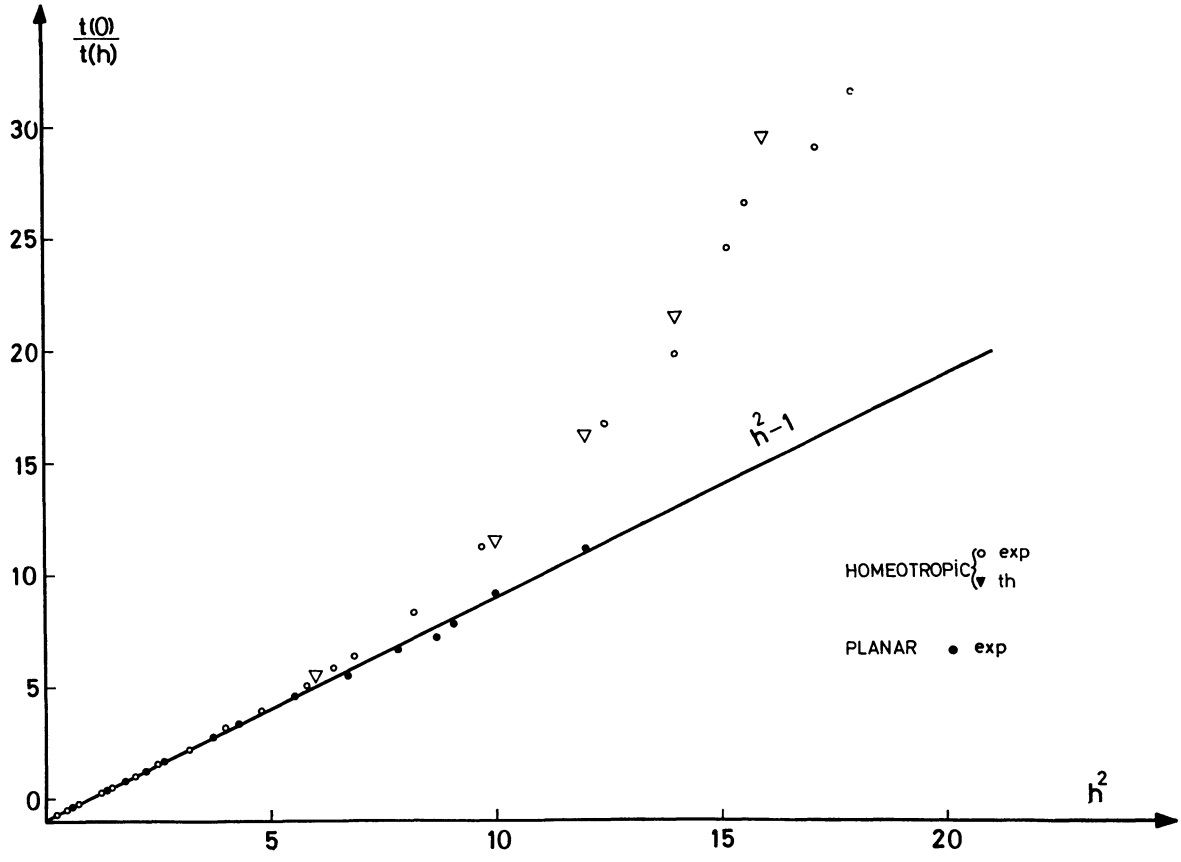

Fig. 14. — The inverse of the time constant, measured optically (see Fig. 3), for upward field ($h_1 > 1$) and downward field ($h_2 < 1$) experiments follow accurately $a\ (h - 1)$ variation in geometry I. The experimental points are normalized to the value for $h = 0$.

to vary with h typically only when $h^2 > 5$. The difference in behavior between the planar case (where $\gamma_1^*(h) = \gamma_1$ remains constant) and the homeotropic case is clearly seen on figure 15 : The $(h^2 - 1)$ law is always obeyed for geometry I whereas the homeotropic results show a strong deviation from the quadratic behavior towards shorter time constants (smaller viscosity $\gamma_1^*(h)$) for larger fields. We have also plotted the corrected calculated form (IV.1) using the variation of $\gamma_1^*(h)/\gamma_1$ which was given on figure 7*b*. This form agrees with the experimental data very well. It gives a very spectacular and quantitative proof of the effect of back flow in a system with solid boundaries. Additional data with different boundary conditions would be desirable. For example, in a LC film with a free surface, relaxing a boundary condition on V_x should lead to an even stronger reduction of the viscosity in the homeotropic geometry.

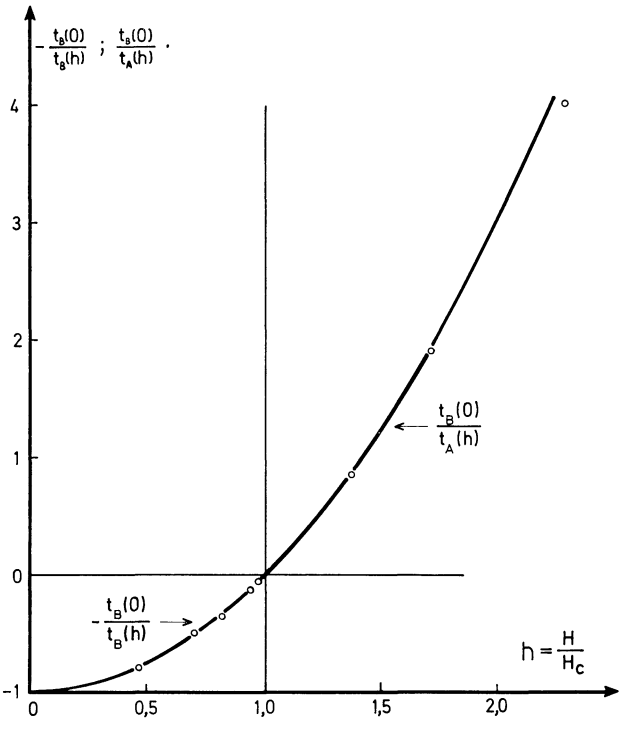

FIG. 15. — The planar results of figure 14 plotted in a h^2 scale indicate no deviation from a parabolic behavior. In geometry III, the deviation from a parabolic variation for large fields, $h^2 > 5$, is related to the decrease of the effective viscosity $\gamma_1^*(h)$ and provides a spectacular demonstration of the back flow effects.

4.2.2 *Viscosity coefficient.* — The viscosity γ_1^* $(h = 0)$ is obtained from the formula :

$$\gamma_1^*(0) = 2\,\tau_B(0)\,\chi_A\,H_c^2 \qquad \text{(IV.2)}$$

which requires measurements of H_c and $\tau_B(0)$ (we have used the values of χ_A given by Gasparoux *et al.* [17] χ_a (27 °C) $\sim 1.1 \times 10^{-7}$ cgs). An accurate determination of $\tau_B(0)$, when a field is suppressed, is given from a plot of Log N versus time (Fig. 16). We observe a linear variation $(0 < N < 10)$ quite accurately and obtain $\tau_B(0)$ with a better than 5 % accuracy. The critical field H_c can be measured from the linear extrapolation of the equilibrium value $N(h)$ towards $N = 0$ (see ref. [1]). This involves very long experiments. An easier determination of H_c is obtained from the field dependence of $\tau(h)$.

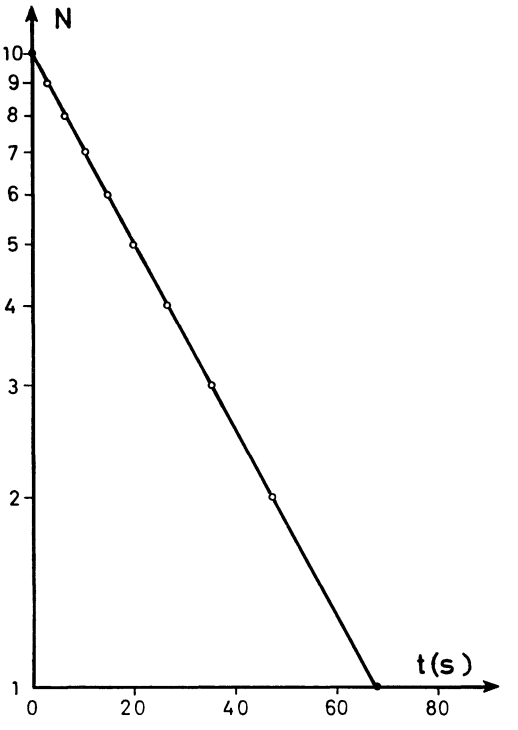

FIG. 16. — A plot of Log N versus t taken from a curve such as given on figure 3 above point B is used to measure the absolute value of γ_1^*.

On figure 17, we show the temperature dependence of $\gamma_1(T)$. This viscosity coefficient was measured for different samples in the planar case $(\gamma_1 = \gamma_1^*)$ and in the homeotropic one

$$\left[\gamma_1 = \frac{\gamma_1^*(0)}{1 - \frac{A}{6}} = \frac{\gamma_1^*(0)}{0.875}\right].$$

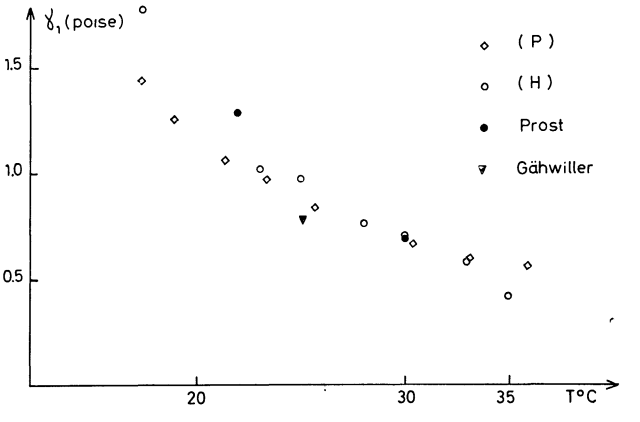

FIG. 17. — Temperature dependence of $\gamma_1(T)$ obtained from experiments in geometry I and III using the method of figure 16. The results are compared with those of reference [11] and [17].

Our data are compared with a value based on flow viscosity by Gähwiller [11] and the temperature dependent data of Prost and Gasparoux [18] who used measurements in a rotating magnetic field. They also agree with those of L. Léger [19] deduced from the motion of walls in a magnetic field. The temperature dependence of $\gamma_1(T)$ is large although we find a smaller dependence than that reported in [17] ; The agreement with the values already published is a further confirmation of the validity of our description. The agreement between planar and homeotropic corrected results is a further proof of the role of back flow effects included in the $(1 - A/6)$ correction in the homeotropic case. However, we feel that this agreement is not as significant a proof as the behavior observed in figure 15 : the accuracy on γ_1 is not better than 10 %. In addition, different LC films were used for the homeotropic and planar studies.

In conclusion, her study of the Freedericksz transition reported in this paper and in reference [1] has led to the study of several static properties (anisotropic heat conductivity, elastic constants) of nematic LC as well as dynamic ones leading to the value of a viscous constant. Back flow effects are described remarkably well by the hydrodynamic Leslie-Ericksen theory. Direct observation of these effects and experiments with different boundary conditions are desirable : along this line, we are now studying the properties of LC films with a normal-nematic interface in the presence of a large enough thermal gradient [20]. Another line of work is the in physico-chemical understanding of the anchoring effects which underlies all this work. Finally, we emphasize that a complementary approach of the dynamics of the Freedericksz transition has been made possible by the work of L. Léger [19] involving the direct observation of nucleation, growth and structure of the domains associated with the application of a field. In our study, we have purposedly studied the properties of only large « crystallites ».

APPENDIX

It might be of interest to outline the analogy between the time constant $\tau(h)$ characterizing the rate of change of the angle $\theta(t)$, which was discussed in the framework of the Landau description of second order phase transition, and a similar time constant $\tau(T/T_c)$ in the Ginsburg-Landau description of superconductors [21], [22]. The latter time gives the rate of change of the superconducting order parameter Δ close to the transition to the normal state ($\Delta \to 0$). In a linear approximation, one has :

$$\frac{\partial \Delta}{\partial t} = \frac{\Delta}{\tau(T/T_c)} .$$

When T is smaller than the critical temperature T_c, this equation describes the exponential growth of the superconducting order (corresponding to case A of our nematic problem) and $\tau(T/T_c) > 0$. The variation of $\tau(T)$ in this domain has been determined indirectly from the magnetic behavior of second kind superconductors and a divergence of $\tau(T)$ as $(1 - T/T_c)^{-1}$ was obtained [21]. The -1 « mean field » exponent obtained in this case as well as in the magnetic field divergence in the LC case comes from the fact that, in the two problems, there exists a large coherence distance ξ. The variation of $\tau(T/T_c)$ for $T > T_c$ corresponding to the exponential decay rate of Δ in the normal state (case B in the LC problems) has also been obtained from proximity effect experiments [22]. It is amusing to note that the variation of $\tau(0)/\tau(T/T_c)$ is strongly analogous to the parabolic variation of $\tau(0)/\tau(h)$ although it is given by a more complex form :

$$\mathrm{Log}\left(\frac{T}{T_c}\right) = \psi\left(\frac{1}{2}\right) - \psi\left(\frac{1}{2} + \frac{\hbar}{4\,\pi k \tau(T)\, T}\right)$$

where $\psi(x) = \Gamma'(x)/\Gamma(x)$ is the digamma function.

The nematic experiments however provide the first direct check of the Landau dynamic description, as the time constant in the superconducting problem is unmeasurably small :

$$\tau(0) \sim \frac{\hbar}{\Delta} \sim 10^{-11}\ \mathrm{s} .$$

References

[1] Pieranski P., Brochard F. and Guyon E., *J. Physique* **7** (1972) 681.

[2] Frank F. C., *Disc. Faraday Soc.*, **251** (1958).
Oseen C. W., *Grans. Faraday Soc.* **29** (1933) 883.

[3] Williams C. and Cladis P. E., *Solid State Commun.* **10** (1972) 357.

[4] Brochard F., Pieranski P. and Guyon E., *Phys. Rev. Lett.* **26** (1972) 1681.

[5] Leslie F. M., *Quart. J. Mech. App. Math.*, **19** (1966), 357.
Ericksen J. L., *Arch. Ratt. Mech. Anal.* **4** (1960) 231 ; **9** (1962) 371.

[6] Groupe d'Orsay des Cristaux Liquides, *J. Chem. Phys.* **51** (1959) 816.

[7] Carslaw H. S., Jaeger J. C., Conduction of heat in solids, Oxford (1959).

[8] Haller I., Huggins H. A., Freiser M. J., *Mol. Cryst. and Liq. Crystals* **16** (1972) 53.

[9] A more detailed description of the experiments is given in Pieranski P., Thèse de 3e cycle, Orsay (1972).

[10] PARODI O., *J. Physique* **31** (1970) 581.
[11] GÄHWILLER C., *Phys. Lett.* **36A** (1971) 311 [the definitions of η_1 and η_2 in this reference are the inverse of ours].
[12] MIESOWICZ M., *Nature* **158** (1946) 27.
[13] MARTINOTY P. and CANDAU S. *Mol. Cryst. and Liq. Crystals*, **14** (1971) 243.
[14] GUYON E., PIERANSKI P., and BROCHARD F., *C. R. Acad. Sci. Paris* **273** (1971) 486.
[15] RAPINI A., Thèse de 3e cycle, Orsay (1970).
[16] LANDAU L. D. and LIFSHITZ E. M., Statistical Physics (Pergamon Press, London 1959), p. 430.
[17] GASPAROUX H., REGAYA B. and PROST J., *C. R. Acad. Sci. Paris* **272** (1971) 1168.
[18] PROST J. and GASPAROUX H., *Phys. Lett.* **36A** (1971) 255.
[19] LÉGER L., to be presented to the 1972 Liquid Crystal Meeting, Kent State University and private communication.
[20] GUYON E., DUBOIS-VIOLETTE E., C. D. Mitescu, *ibid.*
[21] DE GENNES P. G. in Many body Theory, R. Kubo editor, Benjamin New York, 1966, p. 177.
[22] GUYON E., *Adv. Phys.* **15** (1966) 417.
[23] MARTINET A., Thèse Orsay (1967).